Effects of Adhesive and Interphase Characteristics between Matrix and Reinforced Nanoparticle of AA2124/AlN Nanocomposites: Mathematical and Experimental Validation

A. Chennakesava Reddy

Abstract— Interphase around the reinforcement has significant influence on the interfacial stress, displacement and stiffness of composites. In this article two types of RVE models have been implemented using finite element analysis. Aluminum nitride nanoparticles were used as a reinforcing material in the matrix of AA2124 aluminum alloy. It has been observed that the nanoparticle did not overload during the transfer of load from the matrix to the nanoparticle via the interphase due to interphase between the nanoparticle and the matrix. The maximum tensile strengths of AlN/AA2124 nanocomposite have been found 535.40 MPa without interphase and 561.57 MPa with interphase. The transverse modulus has been established lower than the longitudinal modulus of AA2124/AlN nanocomposites. The results obtained from the finite element analysis were validated with mathematically derived and experimental results.

Index Terms— RVE models, AlN nanoparticle, AA2124, finite element analysis, interphase, transverse modulus.

I. INTRODUCTION

During the past several decades composite materials are finding increasing use in a variety of application such as aircraft, automobiles, etc. In the material world, particularly in metal matrix particulate composites, the trend is always to prepare fine powder for the ultimate processing to achieve dense materials with better and useful properties for various applications. More is the fineness; more is the surface area, which increases the reactivity of the material. It is of high importance that the nanoparticles are uniformly dispersed rather than being agglomerated, in order to yield a good property profile in general.

Aluminum nitride (AlN) nanoparticles are enjoying more and more attention now a days, deservedly so as their numerous benefits are being discovered every day. AlN particulate does not deteriorate at high temperature. Owing to its superior properties, AlN particulate is preferred to synthesize composite using Al alloy as matrix. It is important to establish the role of interphase around the AlN nanoparticle on the tensile behavior of AA2124/AlN nanocomposites.

The higher stiffness of ceramic particles can lead to an incremental increase in the stiffness of a composite [1], [2]. One of the major challenges when processing nanocomposites is achieving a homogeneous distribution of reinforcement in the matrix as it has a strong impact on the properties and quality of the material. The current processing methods often generate agglomerated particles in the ductile matrix and as a result they exhibit extremely low ductility [3]. Particle clusters act as crack or decohesion nucleation sites at stresses lower than the matrix yield strength, causing the nanocomposite to fail at unpredictable low stress levels. Possible reasons of particle clustering are chemical binding, surface energy reduction or particle segregation [4], [5], [6]. While manufacturing Al alloy-AlN nanocomposites, the wettability factor is the main concern. Its high surface activity restricts its incorporation in the metal matrix. One of the methods is to add surfactant which acts as a wetting agent in molten metal to enhance wettability of particulates. Several researchers have successfully used several surfactants like Li, Mg, Ca, Zr, Ti, Cu, and Si for the synthesis of nanocomposites [7], [8], [9]. The existence of an interphase region with a higher strength and modulus than the matrix would cause the composites to have superior mechanical properties [10]. Decreasing the interfacial strength can cause the interfacial debonding of particles from the matrix. Interfacial debonding can cause shear yielding of the matrix around the particles.

Composite materials are frequently used to fabricate large structural components. Analyzing large structures on a microstructural level, however, is clearly an inflexible problem. Analysis methods have therefore sought to approximate composite structural mechanics by analyzing a representative section of the composite microstructure, commonly called a Representative Volume Element (RVE). One of the first formal definitions of the RVE was given by Hill [11] who stated that the RVE was 1) structurally entirely typical of the composite material on average and 2) contained a sufficient number of inclusions such that the apparent moduli were independent of the RVE boundary displacements or tractions. Under axisymmetric as well as antisymmetric loading, a 2-D axisymmetric model can be applied for the cylindrical RVE, which can significantly reduce the computational work [12].

The objective of this paper was to establish the effect of presence and absence of interphase as a consequence of with and without wetting criteria of AlN by AA2124 molten metal. The RVE models were used to analyze the AA2124/AlN nanocomposites using finite Element analysis. A homogeneous interphase region was assumed in the models. The results obtained from the finite element analysis were verified with those obtained from the experimentation.

II. THEORETICAL BACKGROUND

The composite material is built up from representative volume elements that are repeated periodically as shown in Fig.1.

Revised Version Manuscript Received on September 04, 2015.

Dr. A. Chennakesava Reddy, Department of Mechanical Engineering, Jawaharlal Nehru Technological University, Hyderabad, India.

Published By:
Blue Eyes Intelligence Engineering
& Sciences Publication Pvt. Ltd.

A. *Determination of Effective Material Properties*

To derive the formulae for deriving the equivalent material constants, a homogenized elasticity model of the square representative volume element (RVE) as shown in Fig.1 is considered. The dimensions of the three-dimensional RVE are 2*a* x 2*a* x 2*a*. The cross-sectional area of the RVE is 2*a* x 2*a*. The elasticity model is filled with a single, transversely isotropic material that has five independent material constants (elastic moduli E_y and E_z, Poison's ratios ν_{xy}, ν_{yz} and shear modulus G_{yz}). The general strain-stress relations relating the normal stresses and the normal stains are given below:

$$\varepsilon_x = \frac{\sigma_x}{E_x} - \frac{\nu_{xy}\sigma_y}{E_y} - \frac{\nu_{xz}\sigma_z}{E_z} \quad (1)$$

$$\varepsilon_y = -\frac{\nu_{yx}\sigma_x}{E_y} + \frac{\sigma_y}{E_y} - \frac{\nu_{yz}\sigma_z}{E_z} \quad (2)$$

$$\varepsilon_z = -\frac{\nu_{zx}\sigma_x}{E_x} - \frac{\nu_{zy}\sigma_y}{E_y} + \frac{\sigma_z}{E_z} \quad (3)$$

Let assume that $\sigma_{xy} = \sigma_{yx}$, $\sigma_{yz} = \sigma_{zy}$ and $\sigma_{zx} = \sigma_{xz}$. For plane strain conditions, $\varepsilon_z = 0$, $\varepsilon_{yz} = \varepsilon_{zx} = 0$ and $\varepsilon_{yz} = \varepsilon_{zx}$. The above equations are rewritten as follows:

$$\varepsilon_x = \frac{\sigma_x}{E_x} - \frac{\nu_{xy}\sigma_y}{E_y} - \frac{\nu_{yz}\sigma_z}{E_z} \quad (4)$$

$$\varepsilon_y = -\frac{\nu_{xy}\sigma_x}{E_y} + \frac{\sigma_y}{E_y} - \frac{\nu_{yz}\sigma_z}{E_z} \quad (5)$$

$$\varepsilon_z = -\frac{\nu_{yz}\sigma_x}{E_z} - \frac{\nu_{yz}\sigma_y}{E_z} + \frac{\sigma_z}{E_z} \quad (6)$$

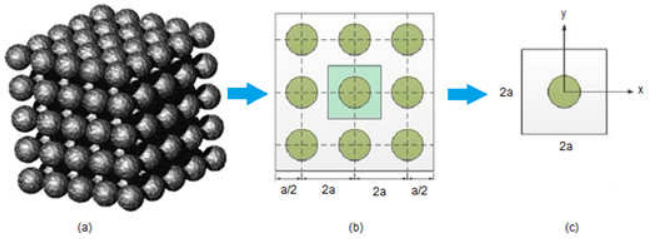

Fig.1. A square RVE containing a nanoparticle.

To determine E_y and E_z, ν_{xy} and ν_{yz}, four equations are required. Two loading cases as shown in Fig.2 have been designed to give four such equations based on the theory of elasticity. For load case (Fig.2a), the stress and strain components on the lateral surface are:

$$\sigma_x = \sigma_y = 0$$

$$\varepsilon_x = \frac{\Delta a}{a} \text{ along } x = \pm a \text{ and } \varepsilon_y = \frac{\Delta a}{a} \text{ along } y = \pm a$$

$$\varepsilon_z = \frac{\Delta a}{a}$$

where Δa is the change of dimension a of cross-section under the stretch Δa in the z-direction. Integrating and averaging Eq. (6) on the plane z = a, the following equation can be arrived:

$$E_z = \frac{\sigma_{ave}}{\varepsilon_z} = \frac{a}{\Delta a}\sigma_{ave} \quad (7)$$

where the average value of σ_z is given by:

$$\sigma_{ave} = \iint \sigma_z(x, y, a)\, dx dy \quad (8)$$

The value of σ_{ave} is evaluated for the RVE using finite element analysis (FEA) results.

Using Eq. (5) and the result (7), the strain along $y = \pm a$:

$$\varepsilon_y = -\frac{\nu_{yz}\sigma_z}{E_z} = -\nu_{yz}\frac{\Delta a}{a} = \frac{\Delta a}{a}$$

Hence, the expression for the Poisson's ratio ν_{yz} is as follows:

$$\nu_{yz} = -1 \quad (9)$$

For load case (Fig.2b), the square representative volume element (RVE) is loaded with a uniformly distributed load (negative pressure), P in a lateral direction, for instance, the x-direction. The RVE is constrained in the z-direction so that the plane strain condition is sustained to simulate the interactions of RVE with surrounding materials in the z-direction. Since $\varepsilon_z = 0$, $\sigma_z = \nu_{yz}(\sigma_x + \sigma_y)$ for the plain stress, the strain-stress relations can be reduced as follows:

$$\varepsilon_x = \left(\frac{1}{E_x} - \frac{1}{E_z}\right)\sigma_x - \left(\frac{\nu_{xy}}{E_y} + \frac{1}{E_z}\right)\sigma_y \quad (10)$$

$$\varepsilon_y = -\left(\frac{\nu_{xy}}{E_x} + \frac{1}{E_z}\right)\sigma_x + \left(\frac{1}{E_x} - \frac{1}{E_z}\right)\sigma_y \quad (11)$$

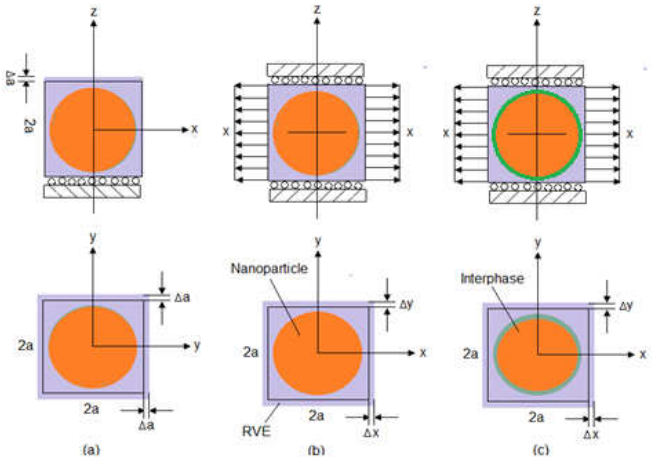

Fig.2. RVE models

For the elasticity model as shown in figure 2b, one can have the following results for the normal stress and strain components at a point on the lateral surface:

$$\sigma_y = 0, \sigma_x = P$$

$$\varepsilon_x = \frac{\Delta x}{a} \text{ along } x = \pm a \text{ and } \varepsilon_y = \frac{\Delta y}{a} \text{ along } y = \pm a$$

where Δx (>0) and Δy (<0) are the changes of dimensions in the x- and y- direction, respectively for the load case shown in figure 2b. Applying Eq. (11) for points along $y = \pm a$ and Eq. (10) for points along $x = \pm a$, we get the following:

$$\varepsilon_y = -\left(\frac{\nu_{xy}}{E_x} + \frac{1}{E_z}\right)P = \frac{\Delta y}{a} \quad (12)$$

$$\varepsilon_x = \left(\frac{1}{E_x} - \frac{1}{E_z}\right)P = \frac{\Delta x}{a} \quad (13)$$

By solving Eqs. (12) and (13), the effective elastic modulus and Poisson's ratio in the transverse direction (xy-plane) as follows:

$$E_x = E_y = \frac{1}{\frac{\Delta x}{Pa} + \frac{1}{E_z}} \quad (14)$$

$$\nu_{xy} = \left(\frac{\Delta y}{Pa} + \frac{1}{E_z}\right)/\left(\frac{\Delta x}{Pa} + \frac{1}{E_z}\right) \quad (15)$$

In which E_z can be determined from Eq. (15). Once the change in lengths along x- and y- direction (Δx and Δy) are determined for the square RVE from the FEA, E_y (= E_x) and ν_{xy} can be determined from Eqs. (14) and (15), correspondingly.

B. *Empirical Models for Elastic Moduli and Strength of Nanocomposites*

The strength of a particulate metal matrix composite depends on the strength of the weakest zone and metallurgical phenomena in it [14], [15]. A new criterion is suggested by the author considering adhesion, formation of precipitates, particle size, agglomeration, voids/porosity, obstacles to the dislocation, and the interfacial reaction of the particle/matrix. The formula for the strength of composite is stated below:

$$\sigma_c = \left[\sigma_m \left\{\frac{1-(v_p+v_v)^{2/3}}{1-1.5(v_p+v_v)}\right\}\right] e^{m_p(v_p+v_v)} + kd_p^{-1/2} \quad (16)$$

Published By:
Blue Eyes Intelligence Engineering
& Sciences Publication Pvt. Ltd.

, $k = E_m m_m / E_p m_p$

where, v_v and v_p are the volume fractions of voids/porosity and nanoparticles in the composite respectively, m_p and m_m are the possion's ratios of the nanoparticles and matrix respectively, d_p is the mean nanoparticle size (diameter) and E_m and E_p is elastic moduli of the matrix and the particle respectively. Elastic modulus (Young's modulus) is a measure of the stiffness of a material and is a quantity used to characterize materials. Elastic modulus is the same in all orientations for isotropic materials. Anisotropy can be seen in many composites. The proposed equations [14], [15] by the author to find Young's modulus of composites and interphase including the effect of voids/porosity as given below:

The upper-bound equation is given by

$$\frac{E_c}{E_m} = \left(\frac{1-v_v^{2/3}}{1-v_v^{2/3}+v_v}\right) + \frac{1+(\delta-1)v_p^{2/3}}{1+(\delta-1)(v_p^{2/3}-v_p)} \quad (17)$$

The lower-bound equation is given by

$$\frac{E_c}{E_m} = 1 + \frac{v_p - v_p}{\delta/(\delta-1)-(v_p+v_v)^{1/3}} \quad (18)$$

where, $\delta = E_p/E_m$.

The transverse modulus is given by

$$E_t = \frac{E_m E_p}{E_m + E_p(1-v_p^{2/3})/v_p^{2/3}} + E_m\left(1 - v_p^{2/3} - v_v^{2/3}\right) \quad (19)$$

The young's modulus of the interphase is obtained by the following formula:

$$E_i(r) = \left(\alpha E_p - E_m\right)\left(\frac{r_i - r}{r_i - r_p}\right) + E_m \quad (20)$$

III. MATERIALS METHODS

The matrix material was AA2124 aluminum alloy. AA2124 contains copper (4.4%Cu), magnesium (1.5%Mg) and manganese (0.6%Mn) as its major alloying elements. The optical microstructure of AA2124 aluminum alloy is shown in Fig. 3(a). The reinforcement material was aluminum nitride (AlN) nanoparticles of average size 100nm. The morphology of AlN nanoparticles is spherical, and they appear as a gray powder as shown in Fig. 3(b). The mechanical properties of materials used in the present work are given in table 1.

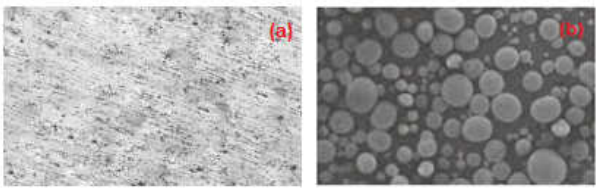

Fig.3. Microstructure of (a) AA2124 and (b) morphology of aluminum nitride nanoparticle.

Table 1. Mechanical properties of AA6061 matrix and AlN nanoparticles

Property	AA2124	AlN
Density, g/cc	2.78	3.26
Elastic modulus, GPa	73.0	330
Ultimate tensile strength, MPa	483	270
Poisson's ratio	0.33	0.24

A. *Preparation of Composite Specimens*

The matrix alloys and composites were prepared by the stir casting and low-pressure die casting process. The volume fractions of AlN reinforcement were 10%, 20%, and 30%. AA2124 matrix alloy was melted in a resistance furnace. The crucibles were made of graphite. The melting losses of the alloy constituents were taken into account while preparing the charge. The charge was fluxed with coverall to prevent dressing. The molten alloy was degasified by tetrachlorethane (in solid form). The crucible was taken away from the furnace; and the melt was treated with sodium modifier. Then the liquid melt was allowed to cool down just below the liquidus temperature to get the melt semi solid state. At this stage, the preheated (500^0C for 1 hour) reinforcement particles and magnesium (Mg) as a wetting agent were added to the liquid melt. The molten alloy and reinforcement particles are thoroughly stirred manually for 15 minutes. After manual steering, the semi-solid, liquid melt was reheated, to a full liquid state in the resistance furnace followed by an automatic mechanical stirring using a mixer to make the melt homogenous for about 10 minutes at 200 rpm. The temperature of melted metal was measured using a dip type thermocouple. The preheated cast iron die was filled with dross-removed melt by the compressed (3.0 bar) argon gas [1], [2].

B. *Heat Treatment*

Prior to the cold rolling of composite samples, a solution treatment was applied at 535^0C for 1 hour, followed by quenching in cold water. The samples were cold rolled to 2% reduction. In a laboratory mill a relatively low strain rate, probably less than 1. Lubricated rolls were used at maximum speed. The strain was calculated from the thicknesses of the test samples before and after rolling process. The strain measurements are defined by:

$$\varepsilon = ln(t_0/t)$$

$$\varepsilon_{vM} = 2/\sqrt{3}\,\varepsilon \quad (21)$$

C. *Tensile Tests*

The heat-treated samples were machined to get flat-rectangular specimens (Fig. 4) for the tensile tests. The tensile specimens were placed in the grips of a Universal Test Machine (UTM) at a specified grip separation and pulled until failure. The test speed was 2 mm/min (as for ASTM D3039). A strain gauge was used to determine elongation.

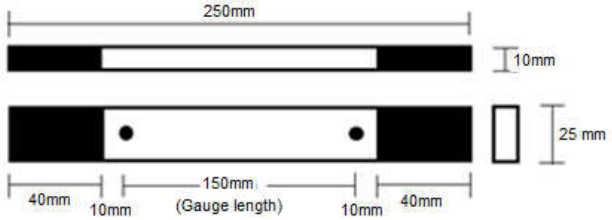

Fig.4. Shape and dimensions of tensile specimen

D. *Optical and Scanning Electron Microscopic Analysis*

An image analyzer was used to study the distribution of the AlN reinforcement particles within the AA2124 matrix. The polished specimens were ringed with distilled water, and etched with a solution (distilled water: 190 ml, nitric acid: 5ml, hydrochloric acid: 3 ml and hydrofluoric acid: 2 ml) for optical microscopic analysis. Fracture surfaces of the deformed/fractured test samples were analyzed with a scanning electron microscope (SEM) to define the

Published By:
Blue Eyes Intelligence Engineering
& Sciences Publication Pvt. Ltd.

macroscopic fracture mode and to establish the microscopic mechanisms governing fracture. Samples for SEM observation were obtained from the tested specimens by sectioning parallel to the fracture surface and the scanning was carried using S-3000N Toshiba SEM.

E. Finite Element Analysis (FEA)

The representative volume element (RVE or the unit cell) is the smallest volume over which a measurement can be made that will yield a value representative of the whole. In this research, a cubical RVE was implemented to analyze the tensile behavior AA2124/AlN nanocomposites. The determination of the RVE's dimensional conditions requires the establishment of a volumetric fraction of spherical nanoparticles in the composite. Hence, the weight fractions of the particles were converted to volume fractions. The volume fraction of a particle in the RVE (VpRVE) is determined using Eq.(22):

$$v_p(\mathrm{RVE}) = \frac{\text{Volume of nanoparticle}}{\text{Volume of RVE}} = \frac{16}{3} \times \left(\frac{r}{a}\right)^3 \quad (22)$$

where, r represents the particle radius and a indicates the diameter of the cylindrical RVE. The volume fraction of the particles in the composite (V_p) is obtained using equation

$$Vp = (w_p/\rho_p)/(w_p/\rho_p + w_m/\rho_m) \quad (23)$$

where ρ_m and ρ_p denote the matrix and particle densities, and w_m and w_p indicate the matrix and particle weight fractions, respectively.

The RVE dimension (a) was determined by equalizing Eqs. (22) and (23). Two RVE schemes namely: without interphase (adhesion) and with interphase were applied between the matrix and the filler. The loading on the RVE was defined as symmetric displacement, which provided equal displacements at both ends of the RVE. To obtain the nanocomposite modulus and yield strength, the force reaction was defined against displacement. The large strain PLANE183 element was used in the matrix and the interphase regions in all the models (table 1). In order to model the adhesion between the interphase and the particle, a COMBIN14 spring-damper element was used. The stiffness of this element was taken as unity for perfect adhesion which could determine the interfacial strength for the interface region.

Table 1. Elements features, applications and size ranges used in RVE modeling

Element code	Plane 183	Contact 172	Combination 14	Target 169
Feature	Quadrilateral-8 nodes	Linear 3 node	Longitudinal spring-damper	Shape complexity
Application	Matrix and interphase	Interface contact	Elastic modeling of adhesion	Contact bodies

For an exact nonlinear solution the converge criteria is also important to set the strain rates of the FEM models based on the experimental tensile tests' setups. Hence, FEM models of different RVEs with various particle contents should have comparable error values. In this respect, the ratio of the tensile test speed to the gauge length of the specimens should be equal to the corresponding ratio in the RVE displacement model. Therefore, the rate of displacement in the RVEs was set to be 0.1 (1/min).

IV. Results and Discussion

Fig. 5 reveals the microstructure of AA2124/AlN nanocomposite wherein the AlN nanoparticles are distributed in the AA2124 matrix uniformly (approximated).

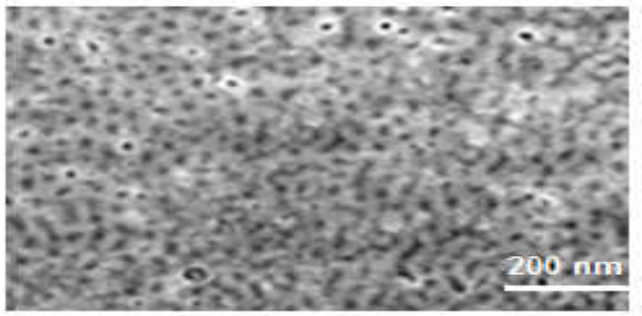

Fig.5. AlN (30%Vp) nanoparticle distribution in AA2124 matrix.

A. Tensile behavior

Fig.6 depicts the tensile strengths of the nanocomposites obtained by FEA (RVE models), author's models, and experimental procedure. The tensile strengths of the nanocomposites did not differ widely, representing that an increase of AlN content in the matrix can increase the tensile strength of the nanocomposite. Author's model includes the effect of voids present in the nanocomposite. The maximum difference between the FEA results without interphase and the experiments results was 23.50 (MPa). This differentiation can be attributed lack of bonding between the AlN nanoparticle and the AA2124 matrix. The maximum difference between the FEA results with interphase and the experiments results was 5.82 (MPa). This discrepancy can be endorsed to the presence of voids in the nanocomposites. In the presence of voids, the interface region between the nanoparticle and the matrix gets stiffened and consequently this leads the slow rate of increasing (or remain constant) the tensile strength with an increase in the nanoparticles content. The results obtained from author's model (with voids) were nearly equal to the experimental values. On the other hand, the deviation of FEA (RVE model) results with the experimental results possibly was as a result of micro-metallurgical factors (such as formation of voids and nanoparticle clustering) that were not considered in the RVE models. However, the nonlinear deformation behavior of the reinforcements and the matrix/reinforcement debonding were considered in the RVE models. These micromechanical factors are important in the large plastic deformation regime.

For 10%, 20% and 30%Vp of AlN in AA2124, without interphase and barely consideration of adhesive bonding between the ALN nanoparticle and the AA2124 matrix, the loads transferred from the AlN nanoparticle to the AA2124 matrix were, respectively, 5.247 (MPa), 24.119 (MPa) and 52.40 (MPa) along the tensile load direction (Fig.7a). The stresses induced in the normal direction to loading were lower than those induced along the load direction (Fig.7b). The compressive stresses were induced in the normal direction of loading. For 10%, 20% and 30%Vp of AlN in AA2124, with interphase and wetting between the ALN nanoparticle and the AA2124 matrix, the loads transferred from the AlN nanoparticle to the AA2124 matrix were, respectively, 9.427 (MPa), 32.936 (MPa) and 79.569 (MPa) along the tensile load direction (Fig.8). Hongwei Zhang et al [16] carried a study improving wettability by adding Mg as the wetting

Published By:
Blue Eyes Intelligence Engineering
& Sciences Publication Pvt. Ltd.

agent. They suggested that the wettability between molten Al-Mg matrix and SiC particles is improved and the surface tension of molten Al-Mg alloy with SiC particle is reduced, and results in homogeneous particles distribution and high interfacial bond strength. For instance, addition of Mg to composite matrix lead to the formation of MgO and $MgAl_2O_3$ at the interface and this enhances the wettability and the strength of the composite [17].

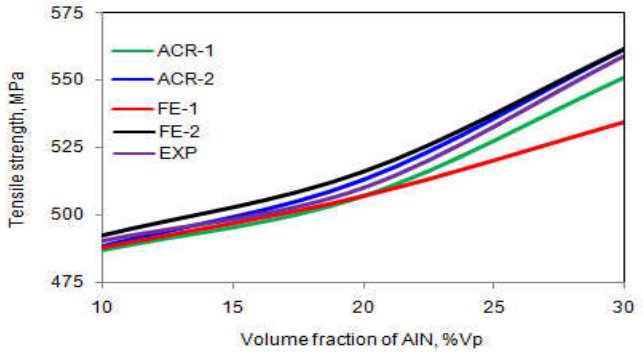

Fig.6. Effect of volume fraction on tensile strength along tensile load direction.

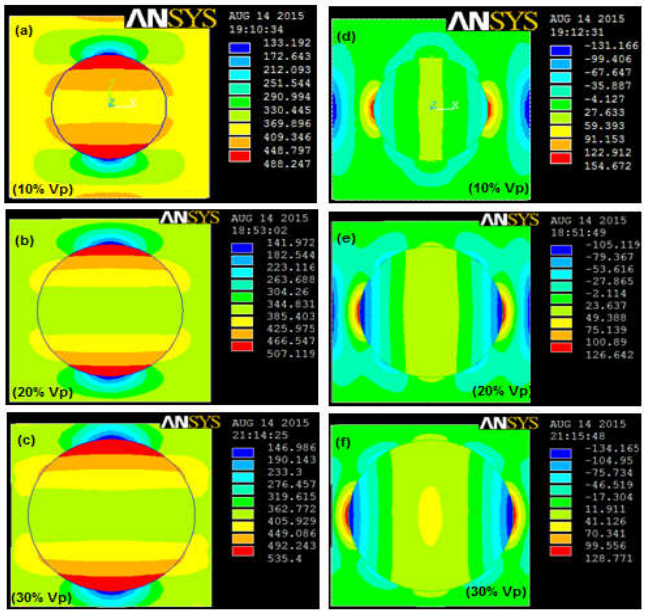

Fig.7. Tensile stresses without interphase: (a) parallel and (b) normal to load direction.

Fig.9 shows the elastic strain contours of the RVE models for the situation involving without interphase. According to Fig.9, the RVE was expanded elastically away from the particle in the direction of the tensile loading. This could increase the contact area between the particle and the matrix in the perpendicular direction to the tensile loading and might decrease the contact area between the particle and the matrix in the direction of the tensile loading. In addition, the deformation was propagated from the matrix to the nanoparticle in the normal direction to the tensile loading. Fig.10 shows the elastic strain contours of the RVE models for the situation involving with interphase. The same kind of trend was observed with the nanocomposites consisting of interphase. The only difference was the propagation of deformation from the matrix to the nanoparticle. The propagation was high with interphase as a consequence of improvement of wettability between the nanoparticle and the matrix. At high volume fractions of AlN, the major strain (tensile) dominated the behavior of deformation (Fig.11). The interphase extended the yielding character of the nano composite. For the homogenization analysis only one cell was analyzed for each volume fraction since the periodicity assumption would give the same result for any number of cells. The local RVE strain was not equal to the average RVE strain but fluctuates about the average RVE strain. The relationship between the average RVE strain and any applied boundary condition was not unique. Increasing the nanoparticle volume fraction can reduce the effect of boundary conditions on the variation of the RVE local strain distribution.

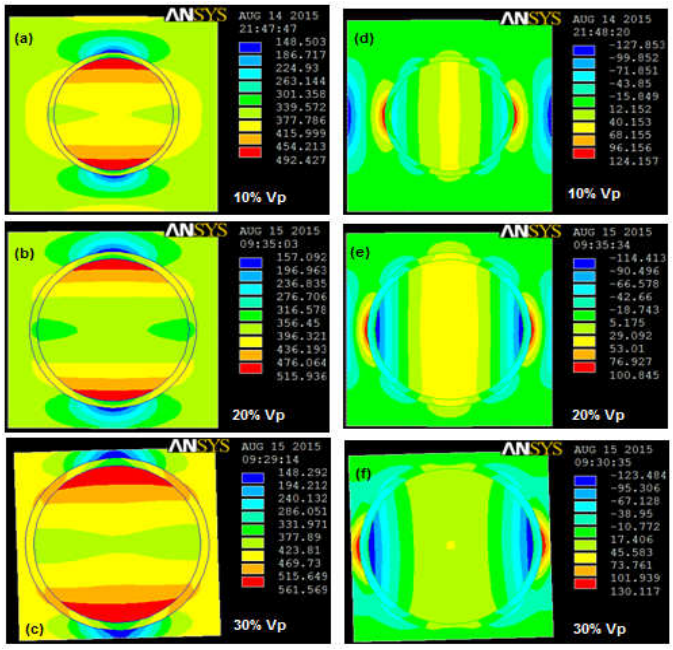

Fig.8. Tensile stresses with interphase: (a) parallel and (b) normal to load direction.

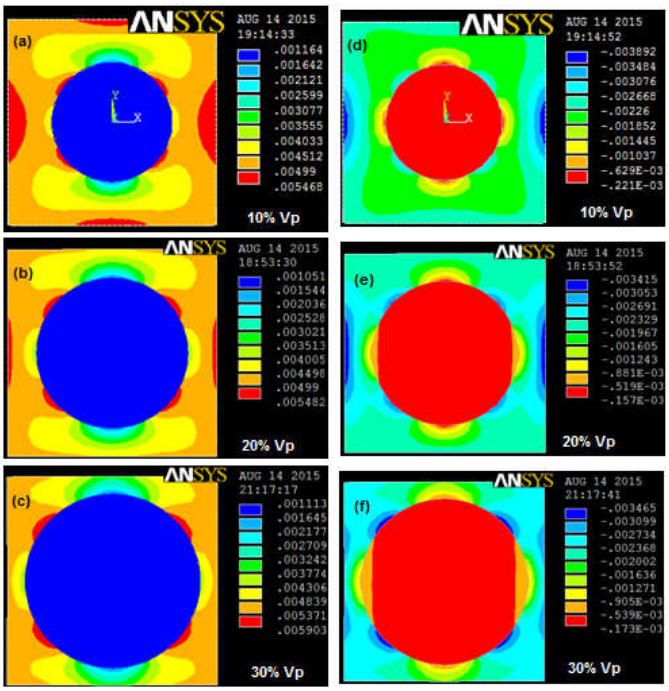

Fig.9. Elastic strain without interphase (a) parallel and (b) normal to load direction.

Published By:
Blue Eyes Intelligence Engineering
& Sciences Publication Pvt. Ltd.

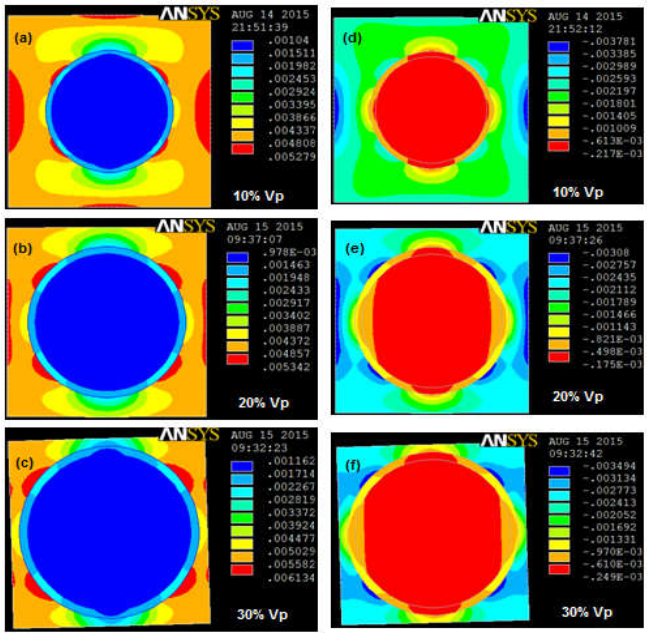

Fig.10. Elastic strain with interphase (a) parallel and (b) normal to load direction.

Table 2 gives the elastic (tensile) moduli of the nanocomposites obtained by FEA and author's models with respect to the volume fraction of AlN nanoparticles. The results of longitudinal moduli obtained FEA were within the limits of Author's models and were closer to the results obtained by the Rule of Mixture. The transverse moduli computed from Eqs. (14) and (15) using FEA data were higher than the results obtained by the author's models and the Rule of Mixture. However, the difference is not too high. The difference in the results obtained by the author's models and to those computed from the Rule of Mixture was due to ignorance of voids in the later case.

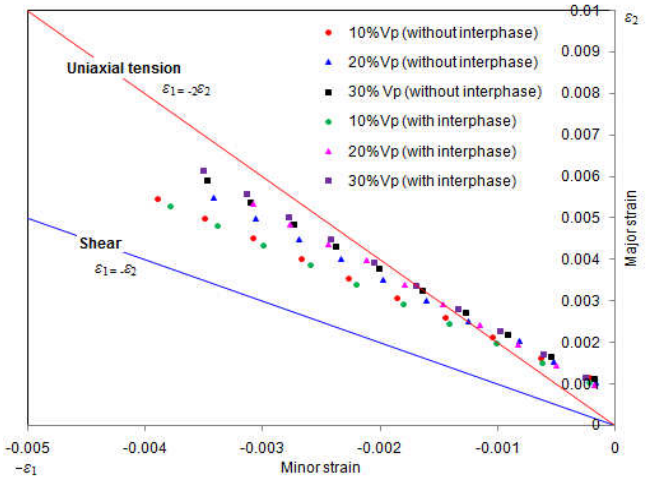

Fig.11. Deformation tendency of AA21124/AlN nano composite

The poisson's ratios v_{zx} (= v_{yz}) is known from Eq. (9). The values of v_{xy} is computed using Eq. (15) from FEA data. Theses results are nearly equal to unity. *Hence, it is proved the assumptions of isotropic conditions while deriving the mathematical models in this paper. The FEA procedure adopted and the the empirical models are also proven acceptable as the results are within permissible limits.* The negative sign indicates the transverse condition as per the conservation of mass or volume during plastic deformation.

Table 12. Elastic moduli of AA2124/AlN nano composite

Source	Criteria	Longitudinal Elastic Modulus, GPa			Transverse Elastic Modulus, GPa		
		Vp = 10%	Vp = 20%	Vp = 30%	Vp = 10%	Vp = 20%	Vp = 30%
FEA	without interphase	89.26	92.54	90.75	89.35	92.64	90.85
FEA	with interphase	93.26	96.62	91.61	93.36	96.72	91.72
Author	upper limit	163.54	179.28	195.19	72.39	77.62	84.94
Author	lower limit	78.21	84.12	90.16	-	-	-
Rule of Mixture		98.79	124.48	150.17	79.27	86.58	95.37

Table 3. Poisson ratios

	Without interphase			With interphase		
Poisson's ratio	Vp = 10%	Vp = 20%	Vp = 30%	Vp = 10%	Vp = 20%	Vp = 30%
v_{xy}	0.9997	0.9996	0.9995	0.9997	0.9995	0.9994
v_{yz}	-1	-1	-1	-1	-1	-1
v_{zx}	-1	-1	-1	-1	-1	-1

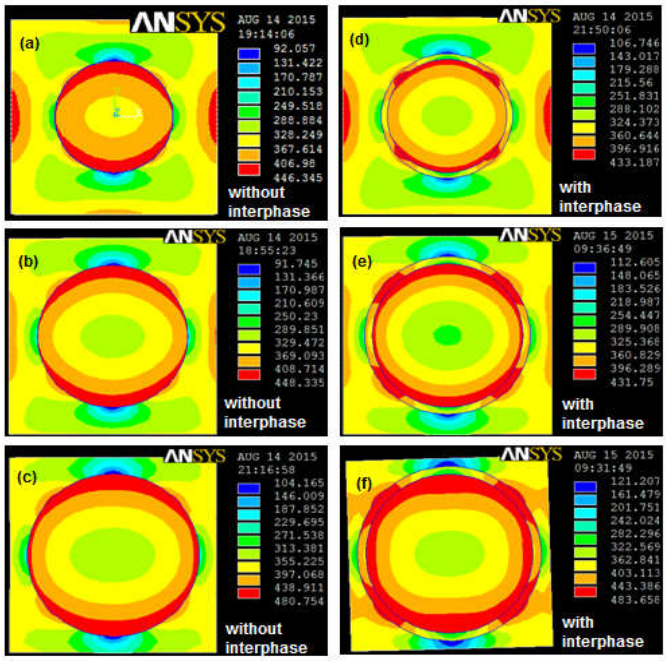

Fig.12. von Mises stress.

Fig.12 shows the variation of von Mises stress in the nanocomposite. The von Mises stress increased with an increase in the volume fraction of AlN. The quality of adhesion at the interface is of crucial importance for the behavior of nanocomposites. The von Mises stresses for the nanocomposites having interphase were lower than those for the nanocomposites without interphase. The adhesion strength at the interface determines the load transfer between the components. Effective stress transfer is the most important factor which contributes to the strength of two-phase composite materials. For poorly bonded particles, the stress transfer at the particle/matrix interface is inefficient. Discontinuities in the form of debonding were observed in the nanocomposites without interphase because of non-adherence of the nano particle to the matrix. However, for composites containing well-bonded particles, addition of particles to a matrix will lead to an increase in strength especially for

Published By:
Blue Eyes Intelligence Engineering
& Sciences Publication Pvt. Ltd.

nanoparticles with high surface areas. Hence, the stress transfer from the matrix to the nanoparticle becomes high for the nanocomposites with interphase.

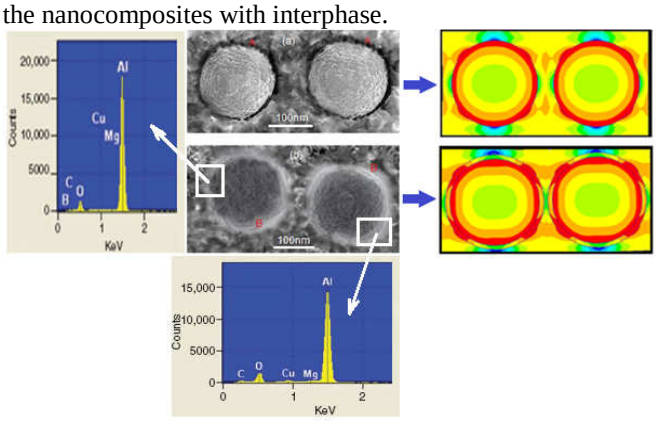

Fig.13. Fracture (a) without interphase and (b) with interphase.

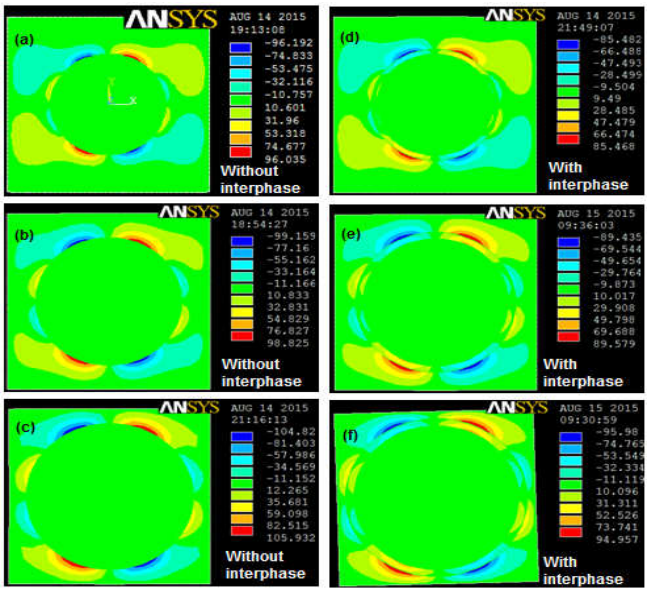

Fig.14. Shear stress: (a) without interphase and (b) with interphase.

B. Fracture

It is observed from Fig.13a that the debonding (A) occurs at the entire periphery of the nanoparticle without interphase between the nanoparticle and the matrix. There is a clear existence of interphase (B) between the AlN nanoparticle and AA2124 matrix (Fig.13b). Mg leads to the formation of MgO and $MgAl_2O_3$ at the matrix-reinforcement interface [17]. The phases Al_2Cu, Al_5Mg_8 were also observed in the microstructures. In static loading conditions, stress equilibrium requires σ_x, σy and τ_{xy} to be continuous regardless of the quality of the interface. Hashin put this imperfect interface model into physical terms for composites [18]. The effect of the interphase is modeled by allowing displacement discontinuities at the 2D interface that are linearly related to the stress in each displacement direction. It is also noticed from Fig.13b that the debonding occurs at the partial periphery of the nanoparticle with interphase between the nanoparticle and the matrix. The elastic stress transfer is analyzed by one-dimensional, shear-lag methods. The shear stresses induced in the nanocomposites with and without interphase are shown in Fig.14. The shear stress induced in the nanocomposite with interphase was lower than that in the nanocomposite without interphase. The rate of change of the stress in the particle to the interfacial shear stress at that point and the particle radius, 'r'.

$$\frac{d\sigma_p}{dx} = -\frac{\tau_i}{r} \qquad (24)$$

In the case of nanocomposites with interphase between the nanoparticle and the matrix, the stress is transferred through shear from the matrix to the particles. Hence, the stress transfer from the matrix to the nanoparticle becomes less for the nanocomposites without interphase resulting high stress in the matrix. Landis and McMeeking [19] assume that the fibers carry the entire axial load, and the matrix material only transmits shear between the fibers. Based on these assumptions alone, it is generally accepted when the fiber volume fraction V_p and the fiber-to matrix moduli ratio E_p/E_m are high. In the present case the elastic moduli of AlN nano particle and AA2124 matrix are, respectively, 73.1 GPa and 330 GPa.

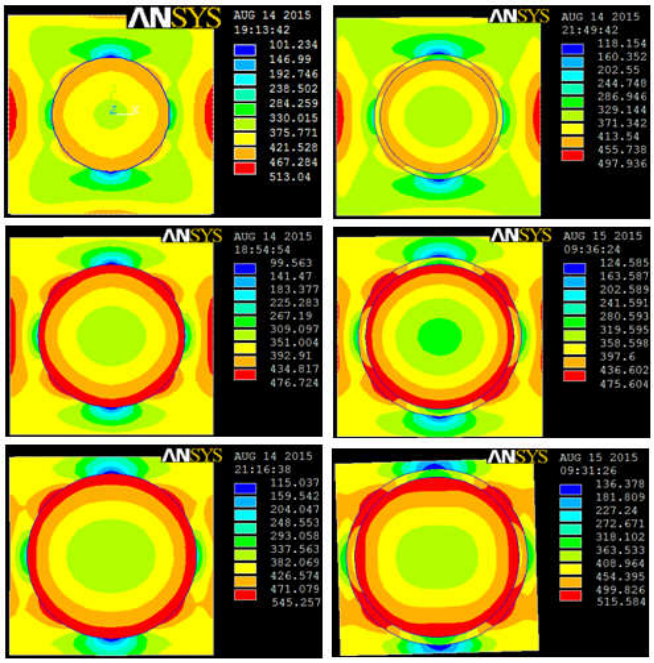

Fig.15. Stress intensity: (a) without interphase and (b) with interphase.

The stress concentration around the nanoparticle can be observed from Fig.15. The stress intensity was higher in the nanocomposite without interphase around the particle than in the nanocomposite with interphase around the particle. The interfacial debonding was high between the particle and the matrix because of local stress concentration around the nanoparticle. The plastic flows were initiated within the matrix and ended at the nanoparticle/matrix interface. Owing to the high stress of the nanoparticles, the plastic deformation becomes concentrated at several locations in the matrix. The localized strain was observed around the particle because of the high load-transfer effect into the particles. The plastic behavior differs considerably with inclusion of interphase between the nanoparticle and the matrix. As the pressure was increased on the RVE model, the plastic strain zone expanded, resulting in a plastic deformation of the interphase between the nanoparticle and the matrix. In the present work the interphase was softer than the matrix and the nanoparticle and the nano particle was stiffer than the matrix.

Published By:
Blue Eyes Intelligence Engineering
& Sciences Publication Pvt. Ltd.

V. CONCLUSION

The RVE models give the trend of phenomenon happening in the nanocomposites. Without interphase and barely consideration of adhesive bonding, the debonding occurs at the particle/matrix interface region in the nanocomposite. Due to interphase between the nanoparticle and the matrix, the nanoparticle is not overloaded during the transfer of load from the matrix to the nanoparticle via the interphase. The tensile strengths obtained by author's model (with voids) and experimental results were nearly equal. In the case of nanocomposites with interphase between the nanoparticle and the matrix, the stress is transferred through shear from the matrix to the particles. The tensile strength and elastic modulus increases with an increase volume fraction of aluminum nitride in the AA2124/AlN nanocomposites. The maximum tensile strength of AlN/AA2124 nanocomposite was 535.40 MPa without interphase; whereas with interphase it was 561.57 MPa.

ACKNOWLEDGEMENTS

The author thanks the University Grants Commission (UGC), New Delhi for sanctioning this major project. The author also thanks the Central University, Hyderabad for providing the SEM images to complete this manuscript.

REFERENCES

1. Chennakesava Reddy, "Mechanical properties and fracture behavior of 6061/SiCp Metal Matrix Composites Fabricated by Low Pressure Die Casting Process," J. Manuf. Technol. Res., vol.1 (3/4), 2009, pp. 273-286.
2. A.Chennakesava Reddy and Essa Zitoun, "Tensile properties and fracture behavior of 6061/Al_2O_3 metal matrix composites fabricated by low pressure die casting process, Int. J. Mater. Sci., vol.6(2), 2011, pp. 147-157.
3. X. Deng and N. Chawla, "Modeling the effect of particle clustering on the mechanical behavior of SiC particle reinforced Al matrix composites," J. Mater. Sci., vol.41, 2006, pp.5731–5734.
4. A.J.Reeves, H.Dunlop and T.W. Clyne, "The effect of interfacial reaction layer thickness on fracture of titanium–SiC particulate composites," Metall. Trans. A, vol.23, 1992, pp.977–88.
5. Kotiveerachari and A. Chennakesava Reddy, "Interfacial effect on the fracture mechanism in GFRP composites,} CEMILAC Conference, Ministry of Defense, India. 1999, 1(b), pp.85-87.
6. Chennakesava Reddy, Analysis of the Relationship Between the Interface Structure and the Strength of Carbon-Aluminum Composites, NATCON-ME, Bangalore, 13-14th March, 2004, pp.61-62.
7. S. Ren, X. Shen, X. Qu and X. He, "Effect of Mg and Si on infiltration behavior of Al alloys pressureless infiltration into porous SiCp preforms," Int. J. Miner. Metall. Mater. Vol.18 (6), (2011, pp.703–708.
8. N. Sobczak, M. Ksiazek, W. Radziwill, J. Morgiel, W. Baliga, and L. Stobierski, "Effect of titanium on wettability and interfaces in the Al/ SiC system," in: Proceedings of the International Conference High Temperature Capillarity, Cracow, Poland, 29 June–2 July 1997.
9. A.M. Davidson and D. Regener, "A comparison of aluminium based metal matrix composites reinforced with coated and uncoated particulate silicon carbide. Compos. Sci. & Technol., vol.60(6), 2000, pp.865-869.
10. M. Romanowicz, "Progressive failure analysis of unidirectional fiber-reinforced polymers with inhomogeneous interphase and randomly distributed fibers under transverse tensile loading," Compos. A, vol.41, 2010, pp.1829-1838.
11. R. Hill, "Elastic properties of reinforced solids: some theoretical principles," J. Mech. Phys. Solids, vol.11, 1963, pp.357-372.
12. Y.J. Liu and X.L. Chen, "Evaluations of the effective material properties of carbon nanotube-based composites using a nanoscale representative volume element," Mech. Mater., vol.35, 2003, pp.69–81.
13. Chennakesava R Alavala, "Finite element methods: Basic concepts and applications," PHI Learning Pvt. Ltd., New Delhi, 2008.
14. Chenna kesava Reddy, "Cause and Catastrophe of Strengthening Mechanisms in 6061/Al_2O_3 Composites Prepared by Stir Casting Process and Validation Using FEA," Int. J. Sci. & Res., vol.4(2), 2015, pp.1272-1281.
15. Chennakesava Reddy, "Influence of Particle Size, Precipitates, Particle Cracking, Porosity and Clustering of Particles on Tensile Strength of 6061/SiCp Metal Matrix Composites and Validation Using FEA," Int. J. Mater. Sci.& Manuf. Eng., vol.42(1), 2015, pp. 1176-1186.
16. Zhengang Liuy, Guoyin Zu, Hongjie Luo, Yihan Liu and Guangchun Yao, "Influence of Mg Addition on Graphite Particle Distribution in the Al Matrix Composites," J. Mater. Sci. & Technol., vol.26 (3), 2010, pp.244-250.
17. Chennakesava Reddy and Essa Zitoun, "Matrix alloys for alumina particle reinforced metal matrix composites," Indian Foundry J., vol.55 (1), 2009, pp.12-16.
18. Z. Hashin, "Thermoelastic Properties of Fiber Composites With Imperfect Interface," Mech. of Mater., vol. 8, 1990, pp. 333-348.
19. C.M. Landis and R.M. McMeeking, "Stress concentrations in composites with interface sliding, matrix stiffness, and uneven fiber spacing using shear lag theory, ". Int. J. Solids Structures, vol.41, 1999, pp. 6289-6313.

AUTHOR PROFILE

Dr. A. Chennakesava Reddy, B.E., M.E (prod). M.Tech (CAD/CAM)., Ph.D (prod)., Ph.D (CAD/CAM) is a Professor in Mechanical Engineering, Jawaharlal Nehru Technological University, Hyderabad. The author has published 256 technical papers worldwide. He is the recipient of best paper awards ten times. He is recipient of Best Teacher Award from the Telangana State, India. He has successfully completed several R&D and consultancy projects. He has guided 14 Research Scholars for their Ph.D. He is a Governing Body Member for several Engineering Colleges in Telangana. He is also editorial member of Journal of Manufacturing Engineering. He is author of books namely: FEA, Computer Graphics, CAD/CAM published by PHI, Fuzzy Logic and Neural Networks published by New Age International, and Instrumentation and Controls published by Cengage Learning. Number of citations are 578. The total impact factors are 208.1339. Average Cites per Paper is 2.2578. The author's h-index and i10-index are 18 and 21, respectively. His research interests include Fuzzy Logic, Neural Networks, Genetic Algorithms, Finite Element Methods, CAD/CAM, Robotics and Characterization of Composite Materials and Manufacturing Technologies.

Published By:
Blue Eyes Intelligence Engineering
& Sciences Publication Pvt. Ltd.